Journal of
Synchrotron
Radiation

ISSN 0909-0495

Received 3 December 2007
Accepted 4 February 2008

Element-specific microtomographic imaging of *Drosophila* brain stained with high-*Z* probes

Ryuta Mizutani,[a]* Akihisa Takeuchi,[b] Genta Akamatsu,[a] Kentaro Uesugi[b] and Yoshio Suzuki[b]

[a]Department of Applied Biochemistry, School of Engineering, Tokai University, Kitakaname 1117, Hiratsuka, Kanagawa 259-1292, Japan, and [b]Research and Utilization Division, JASRI/SPring-8, Kouto 1-1-1, Sayo, Hyogo 679-5198, Japan. E-mail: ryuta@keyaki.cc.u-tokai.ac.jp

An application of X-ray microtomography to the *Drosophila* adult brain stained with colloidal gold and a platinum compound is described. The transparency of biological tissue to hard X-rays enables tomographic visualization of the three-dimensional structure of tissue entrails. Each high-*Z* element was visualized as a three-dimensional structure from the difference absorption coefficient image at the corresponding L_{III} absorption edge. The cortex of the optic lobe was selectively visualized by the specific adsorption of colloidal gold. The entire structure revealed by the platinum impregnation allowed the anatomical assignment of the gold-stained structures. Selective staining and specific visualization of biological tissues at micrometer resolution should elucidate the three-dimensional cellular organization essential for the understanding and application of biological microstructures.

Keywords: micro-CT; microcontrasting; central nervous system; nanoparticle.

1. Introduction

Biological tissues are mainly composed of light elements. Their transparency to hard X-rays enables radiographic analysis of tissue entrails. However, they produce little contrast in a hard X-ray transmission image. The contrast can be enhanced by using soft X-rays, but these are significantly absorbed even by water and air, so analysis has consequently been performed in a vacuum. The application of phase-contrast techniques for developing the interferometric images has been reported (Snigirev *et al.*, 1995; Momose *et al.*, 1996; Wilkins *et al.*, 1996). The interferometric image of soft tissue gives the distribution of electron densities, while the image contrast has no inherent relationship with the cellular organization or biological functions. Therefore, the three-dimensional structure of soft tissues should be selectively visualized by contrasting each biological constituent.

In clinical diagnosis, luminal structures of a living body are visualized by using X-ray contrast media. These contrast media contain high-*Z* elements, such as iodine or barium, that absorb X-rays efficiently. We have recently shown that the neuronal structure of the *Drosophila* larvae central nervous system (CNS) can be visualized by contrasting every neuron using the metal impregnation method (Mizutani *et al.*, 2006). In conjunction with high-resolution X-ray computed tomography (Uesugi *et al.*, 2001; Takeuchi *et al.*, 2002), hereafter called micro-CT, metal microcontrasting has revealed the entire three-dimensional structure of the *Drosophila* larvae CNS (Mizutani *et al.*, 2007) and the neuronal structure of the human frontal cortex (Mizutani *et al.*, 2008).

Multiple labeling with fluorescent probes has been widely used in optical microscopic studies (Conchello & Lichtman, 2005). The location of a probe is determined from its specific fluorescence. Similarly, the native distribution of metal elements can be visualized by observing absorption or fluorescence images around the X-ray absorption edge (McNear *et al.*, 2005). If the high-*Z* element probe is selectively adsorbed at a specific region, we can determine the three-dimensional location of a biological constituent associated with the probe adsorption in the micro-CT image.

Selective staining using colloidal gold conjugates has been reported for histological analysis of biological tissues. While the colloidal probe can be visualized by the micro-CT analysis, unstained tissue composed of light elements cannot be observed in radiographs. Therefore, tissues should be stained with another high-*Z* element to specify the location of the colloidal probe in the overall structure. This counterstaining technique facilitates the visualization of the whole image, which can be used as a reference structure for the anatomical assignment of the selectively stained regions.

Therefore, multiple staining should be performed to analyze the functional microstructure of biological tissues. Here, we report an element-specific micro-CT analysis of the CNS of adult *Drosophila melanogaster* stained with gold and platinum probes. The cortex of the optic lobe showed a specific affinity for colloidal gold and gave localized gold densities. The nerve

tissue was further counterstained by the reduced silver staining method (Mizutani *et al.*, 2007) using a platinum compound, giving the overall structure of the *Drosophila* CNS. The three-dimensional microstructure visualized by these high-Z probes revealed the nerve tissue structure responsible for the CNS functions.

2. Materials and methods

2.1. Colloidal gold

Colloidal gold was prepared as described previously (Kanayama & Kitano, 2000) with slight modifications. An aqueous solution of hydrogen tetrachloroaurate (0.01%, 10 ml) was boiled in a microwave oven for 5 min. After the addition of 250 µL solution containing 1% sodium citrate, the mixture was allowed to cool to room temperature, giving a ruby-colored colloid solution. The average hydrodynamic diameter of colloidal gold obtained by this method has been reported to be 20 nm.

2.2. *Drosophila* CNS

Wild-type *D. melanogaster* Canton-S were raised on standard cornmeal-molasses fly food and kept at 293 K. Adult fly CNSs were dissected and fixed for 60 min in a solution containing 85% ethanol, 5% acetic acid and 4% formaldehyde. After being washed with ethanol, the CNSs were progressively hydrated in 90%, 70%, 50% and 30% ethanol and then in distilled water. These rehydrated CNSs were immersed in the colloidal gold solution (pH 4.0) at 277 K for 72 h. The samples were then washed with water twice and subjected to modified reduced-silver staining (Mizutani *et al.*, 2007). The silver impregnation was performed for 15 h at 310 K using 0.04% silver nitrate solution containing 0.75% pyridine and 25 mM sodium borate (pH 8.4). The CNS samples were then developed for 10 min at 298 K in a solution containing 1% hydroquinone and 10% sodium sulfite. After being washed with distilled water twice, the samples were toned with 2% ammonium tetrachloroplatinate for 50 min under the irradiation of 350 nm UV light. After washing, the samples were immersed sequentially in 2% oxalic acid for 10 min and 5% sodium thiosulfate for 5 min, with washes in distilled water between immersions. After removal of the residual sodium thiosulfate by washing, the samples were dehydrated in an ethanol series and transferred to *n*-butyl glycidyl ether, and then to Petropoxy 154 epoxy resin (Burnham Petrographics, ID). Nylon loops like those used in protein cryocrystallography (Teng, 1990) were used for mounting the sample for the radiographic analysis. The epoxy resin was rigidified by 363 K treatment for 16 h.

2.3. Micro CT

Projection-CT analysis was performed using the BL20XU beamline of SPring-8 (Hyogo, Japan). Transmission radiographs were recorded using a CCD-based X-ray imaging detector (AA50 and C4880-41S, Hamamatsu Photonics). The field of view and effective pixel size of the image detector are 1.00 mm × 0.65 mm and 0.50 µm × 0.50 µm, respectively. Each image was acquired with a rotation step of 0.10° and an exposure time of 300 ms. In total, three data sets were acquired using monochromatic X-rays corresponding to wavelengths above the Au L_{III} edge (12.000 keV) and Pt L_{III} edge (11.700 keV) and beneath these edges (11.400 keV). The spatial resolution of the three-dimensional structure has been estimated to be 1.0 µm in each direction (Uesugi *et al.*, 2001).

The convolution back-projection method using a Chesler-type filter was used for tomographic reconstruction (Uesugi *et al.*, 2001). Reconstructed images were further processed using the program suite *rmsd* (Nakano *et al.*, 2006) to calculate difference absorption tomograms. The gold distribution image was prepared by subtracting the three-dimensional distribution of linear absorption coefficients at 11.7 keV from that at 12.0 keV. The platinum image was prepared by subtracting the 11.4 keV image from the 11.7 keV image. Volume-rendered figures of the obtained three-dimensional structures were produced using the VG Studio MAX (Volume Graphics GmbH, Germany). CT densities were rendered by the maximum projection method.

The data acquisition conditions are summarized in Table 1.

Table 1
Tomographic data acquisition conditions.

Beamline	BL20XU
Pixel size (µm)	0.50
Spatial resolution (µm)	1.0
Viewing field (mm)	1.00 × 0.65 (width × height)
Rotation/frame (°)	0.10
Exposure/frame (ms)	300
Frame/dataset	1800
Dataset acquisition time (min)	33

3. Results and discussion

The adult *Drosophila* CNS consists of the right and left optic lobes and the central brain (*e.g.* Rein *et al.*, 1999). The stained tissue is clearly distinguishable from the epoxy-resin surroundings (Fig. 1), indicating that colloidal gold adsorption along with platinum counterstaining can be used for radiographic observation of the nerve tissue.

The three-dimensional gold distribution (Fig. 1*a*) revealed that the colloidal gold was specifically adsorbed at the cortex of optic lobes and some surrounding tissue attached to the surface of the central brain. The gold distribution at the optic lobe cortex coincides with the optical microscope observation that each end of the optic lobe was stained dark red by the colloidal gold treatment. Colloid staining was performed by the simple procedure of just immersing the nerve tissue in the colloid solution. Therefore, specific adsorption of colloidal gold indicates the simultaneous affinity of colloidal gold for the optic lobe cortex. It has been reported that the charged gold surface shows a high electrostatic affinity for cell and tissue components (Behnke *et al.*, 1986). Nucleophilic groups can covalently bind to colloidal gold (Kirk & Bohn, 2004), suggesting that nucleophilic moieties such as cysteinyl sulf-

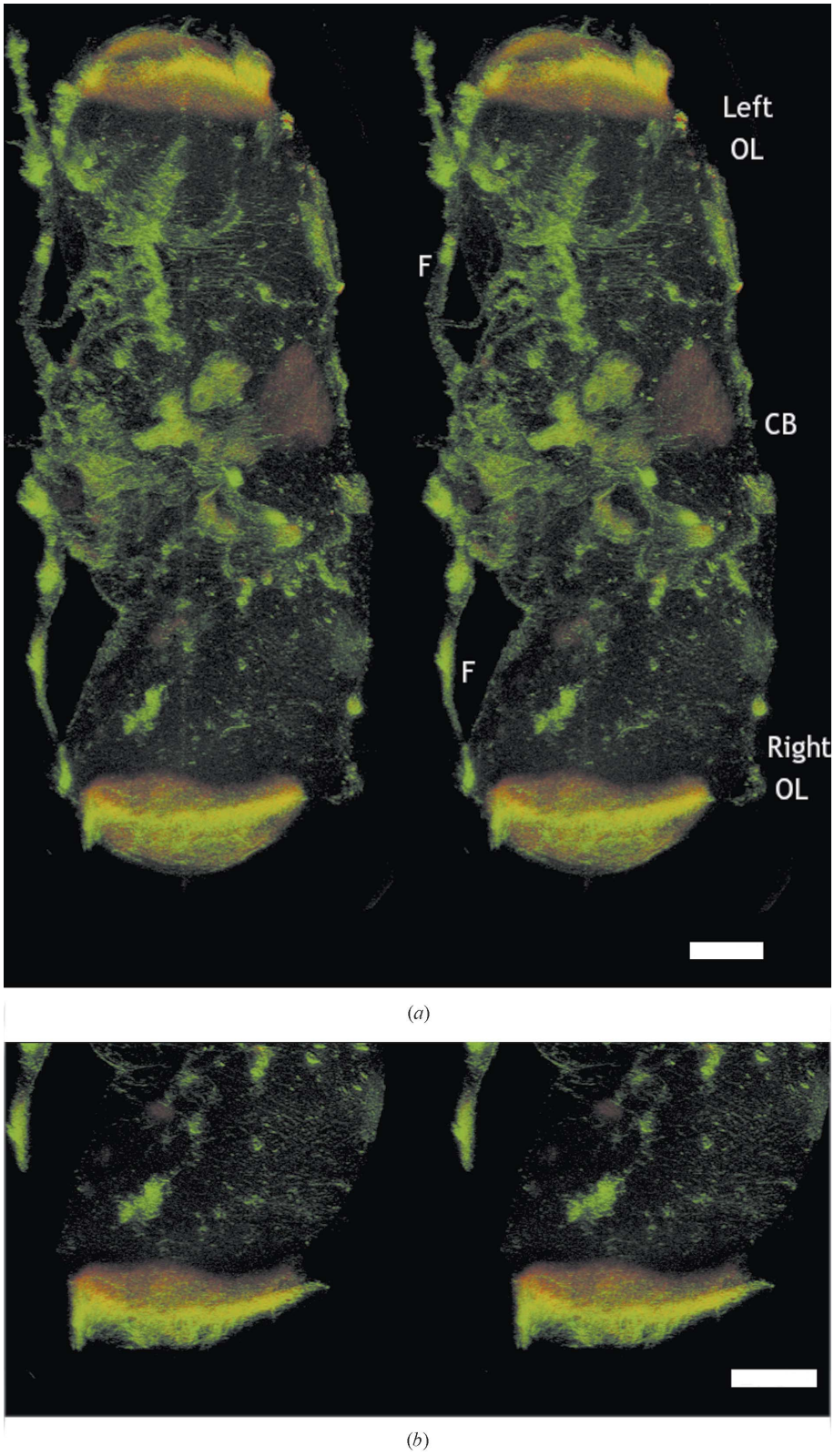

Figure 1
Stereo representations of adult *Drosophila* CNS structures analyzed at the Au L_{III} absorption edge and Pt L_{III} edge. Gold and platinum distributions are superposed and colored red and green, respectively. (*a*) The entire structure. (*b*) A cutaway view of the right optic lobe sectioned at a middle coronal plane. Dorsal is to the right. CT densities are rendered from low level (corresponding to a difference linear absorption coefficient of +5.8 cm^{-1}) to high level (+17.3 cm^{-1}). CB, central brain; F, nerve fiber; OL, optic lobe. Scale bar: 50 µm.

hydryl groups would be localized at the optic lobe cortex and the surrounding tissue in the adult *Drosophila* CNS.

The reduced silver impregnation using tetrachloroplatinate mainly visualizes neural cell bodies in the tissue cortex and nerve fibers linked to peripheral organs (Fig. 1*a*). The platinum image of the overall CNS structure facilitates the anatomical assignment of structures selectively stained with colloidal gold. Localized platinum densities reflect differences in the affinity of each tissue constituent for the platinum compound. Optic lobes were also visualized in the platinum image. This would be due to the platinum adsorption on colloidal gold surfaces. Colloidal gold concentrated in the optic lobe cortex can be coated with silver (Danscher *et al.*, 1994), which is then replaced with platinum through the staining procedure.

The colloidal gold was adsorbed at the tissue cortex. Therefore, the overall surface structure visualized by the platinum impregnation rather than neuropil networks in the tissue medulla is appropriate as a counterstained image. A cutaway view of the right optic lobe (Fig. 1*b*) shows that colloidal gold penetrated 10–30 µm deep from the tissue surface. The optic lobe consists of four neuropil regions: the lamina, medulla, lobula and lobula plate. In the present dissection procedure, the lamina was almost removed along with the eye and head capsule. Therefore, the colloidal gold observed in the micro-CT image corresponds to medulla surfaces or residual lamina of the optic lobes.

Confocal optical microscopy is the primary method for visualizing three-dimensional structures of biological systems (Conchello & Lichtman, 2005). The neuronal structures of the *Drosophila* adult brain have been visualized using confocal microscopy (*e.g.* Lee *et al.*, 2000). However, absorbance at emission or excitation wavelengths interferes with the detection of fluorescence elicited from the internal architecture. Although the maximum spatial resolution of an optical microscope is estimated to be about half the observation wavelength (200–300 nm), the

observation depth is typically limited to 100 μm in confocal microscopy. This causes difficulties in three-dimensional reconstruction of the entire optical image of thick samples. Thus, confocal microscopy is mainly used for imaging sectioned samples labeled with highly selective probes. Optical computed tomography and ultramicroscopy have recently been applied to the three-dimensional analysis of biological tissues (Alanentalo *et al.*, 2007; Dodt *et al.*, 2007), although the internal structure of opaque samples cannot be observed using visible light. While magnetic resonance imaging provides a non-invasive mapping of neural activity (Yu *et al.*, 2005), cellular structures are not visualized owing to the limited spatial resolution.

In contrast, the transparency of biological tissue to hard X-rays enables microcontrasted three-dimensional CT analysis (Mizutani *et al.*, 2007, 2008). The viewing field and spatial resolution of the micro-CT analysis can be varied depending on the pixel size, image dimensions and X-ray optics. In the present study, the three-dimensional structure in a cylindrical region 1.00 mm in diameter × 0.65 mm in height was reconstructed from the 2000 × 1300 pixel projection images with effective pixel size of 0.5 μm. Although the spatial resolution of the reconstructed structure from projection images has been estimated to be 1.0 μm (Uesugi *et al.*, 2001), application of the zone plate optics (Takeuchi *et al.*, 2002) would enable the structure determination at a higher resolution. We have reported a radiographic analysis of nerve tissue at 160 nm resolution (Mizutani *et al.*, 2007) visualizing the neuronal structures. Selective microcontrasting CT analysis at this higher resolution enables functional analysis of the neuronal network from the three-dimensional microstructure of the nerve tissue.

Biological tissues consist of cells, which can be classified into a number of types by their biological functions, *e.g.* neurons and glias in the nerve tissue. Each cell possesses specific markers from which the cellular properties can be identified. Selective staining of the specific markers using antibody conjugates allows the visualization of the three-dimensional distribution of each cell type, providing a microstructural body plan of tissues and organs. The three-dimensional structures of industrial products have been used in rapid prototyping of constituent parts by three-dimensional printing (Sachs *et al.*, 1992). Therefore, if three-dimensional printing techniques for biological cells are established, an artificial organ could be microfabricated from the three-dimensional structure revealed by micro-CT analysis.

The synchrotron radiation experiments were performed at SPring-8 with the approval of the Japan Synchrotron Radiation Research Institute (JASRI) (proposal Nos. 2007A1844 and 2007B1102).

References

Alanentalo, T., Asayesh, A., Morrison, H., Lorén, C. E., Holmberg, D., Sharpe, J. & Ahlgren, U. (2007). *Nat. Methods*, **4**, 31–33.
Behnke, O., Ammitzbøll, T., Jessen, H., Klokker, M., Nilausen, K., Tranum-Jensen, J. & Olsson, L. (1986). *Eur. J. Cell Biol.* **41**, 326–338.
Conchello, J. A. & Lichtman, J. W. (2005). *Nat. Methods*, **2**, 920–931.
Danscher, G., Stoltenberg, M. & Juhl, S. (1994). *Neuropathol. Appl. Neurobiol.* **20**, 454–467.
Dodt, H.-U., Leischner, U., Schierloh, A., Jährling, N., Mauch, C. P., Deininger, K., Deussing, J. M., Eder, M., Zieglgänsberger, W. & Becker, K. (2007). *Nat. Methods*, **4**, 331–336.
Kanayama, N. & Kitano, H. (2000). *Langmuir*, **16**, 577–583.
Kirk, J. S. & Bohn, P. W. (2004). *J. Am. Chem. Soc.* **126**, 5920–5926.
Lee, T., Marticke, S., Sung, C., Robinow, S. & Luo, L. (2000). *Neuron*, **28**, 807–818.
McNear, D. H. Jr, Peltier, E., Everhart, J., Chaney, R. L., Sutton, S., Newville, M., Rivers, M. & Sparks, D. L. (2005). *Environ. Sci. Technol.* **39**, 2210–2218.
Mizutani, R., Hara, T., Takeuchi, A., Uesugi, K. & Suzuki, Y. (2006). *Proceedings of the Fifth East Asian Biophysics Symposium*, S388.
Mizutani, R., Takeuchi, A., Hara, T., Uesugi, K. & Suzuki, Y. (2007). *J. Synchrotron Rad.* **14**, 282–287.
Mizutani, R., Takeuchi, A., Uesugi, K., Ohyama, M., Takekoshi, S., Osamura, R. Y. & Suzuki, Y. (2008). *Brain Res.*, doi:10.1016/j.brainres.2008.01.029.
Momose, A., Takeda, T., Itai, Y. & Hirano, K. (1996). *Nat. Med.* **2**, 473–475.
Nakano, T., Tsuchiyama, A., Uesugi, K., Uesugi, M. & Shinohara, K. (2006). *Slice: softwares for basic 3-D analysis*, http://www-bl20.spring8.or.jp/slice/.
Rein, K., Zöckler, M. & Heisenberg, M. (1999). *Curr. Biol.* **9**, 93–96.
Sachs, E., Cima, M., Williams, P., Brancazio, D. & Cornie, J. (1992). *J. Eng. Indust.* **114**, 481–488.
Snigirev, A., Snigireva, I., Kohn, V., Kuznetsov, S. & Schelokov, I. (1995). *Rev. Sci. Instrum.* **66**, 5486–5492.
Takeuchi, A., Uesugi, K., Takano, H. & Suzuki, Y. (2002). *Rev. Sci. Instrum.* **73**, 4246–4249.
Teng, T.-Y. (1990). *J. Appl. Cryst.* **23**, 387–391.
Uesugi, K., Suzuki, Y., Yagi, N., Tsuchiyama, A. & Nakano, T. (2001). *Nucl. Instrum. Methods*, A**467–468**, 853–856.
Wilkins, S. W., Gureyev, T. E., Gao, D., Pogany, A. & Stevenson, A. W. (1996). *Nature (London)*, **384**, 335–338.
Yu, X., Wadghiri, Y. Z., Sanes, D. H. & Turnbull, D. H. (2005). *Nat. Neurosci.* **8**, 961–968.